Fringing-Field Effects on High-Resolution Liquid Crystal Microdisplays

Kuan-Hsu Fan-Chiang, Shin-Tson Wu, *Fellow, IEEE*, and Shu-Hsia Chen

Invited Paper

***Abstract*—Fringing-field effects on high-resolution liquid crystal microdisplay devices, including the reflection-type liquid-crystal-on-silicon (LCOS) and transmission-type poly-silicon thin-film-transistor liquid crystal displays are simulated by the beam propagation method. The electro-optic performances of six commonly used liquid crystal modes are analyzed by the two-dimensional optical simulator. The vertically aligned (VA) cell exhibits the highest contrast ratio, but its fringing-field effect is severe. A circularly polarized light illuminated LCOS device is presented to eliminate the fringing-field effect of the VA cell. Both simulated and confirming experimental results show that the long-standing problems of poor sharpness, low brightness, and slow transition time of the VA cell can be overcome by using a circularly polarized light.**

***Index Terms*—Beam-propagation method (BPM), fringing-field effect, liquid-crystal-on-silicon (LCOS), projection display.**

I. Introduction

HIGH resolution liquid-crystal-on-silicon (LCOS) devices have been widely used for rear projection and near-the-eye virtual displays [1]. Due to the high electron mobility of crystalline silicon, LCOS devices can be fabricated with a very small pixel size ($\sim$10 μm) and submicron inter-pixel gap. When the adjacent pixels are operated at different voltages, the LC directors near the pixel edges are distorted by the lateral component of the fringing field, which significantly degrades the electro-optic performance of the device [2]. In addition, as the pixel gap becomes comparable to the incident light wavelength, diffraction effect can cause severe light loss [3].

In this review paper, we investigate the fringing-field effects on the reflective LCOS and transmissive LC microdisplay devices. In reflective displays, six commonly used LC modes: normally-white (NW) 90° mixed-mode twisted-nematic (MTN) cell [4], NW 45°-MTN [5], normally-black (NB) 45° TN cell [6], NW film-compensated homogenous (FCH) cell [7], NB vertically aligned (VA) cell [8], and NB finger-on-plane (FOP) cell [9] are simulated and results compared. In the transmissive LC microdisplays using poly-silicon thin-film-transistor liquid crystal displays (TFT-LCDs), the TN and VA cells are compared. To simulate the electro-optic performances of the LCOS devices, the extended beam-propagation method (BPM) [3], is employed. Unlike the matrix-type (e.g., Jones matrix) methods [10]–[12], the BPM takes light scattering and diffraction effects into consideration. Furthermore, its computation speed is faster than that of the complex finite-difference time-domain (FDTD) method [13]–[15].

In order to eliminate the fringing-field effects while keeping high contrast ratio, a circularly polarized light illuminated vertically aligned (CPVA) cell is introduced [16]. Both simulated and experimental results confirm that the CPVA device has effectively overcome the fringing field problems.

This review paper is arranged in the following sequence: in Section II, the extended beam propagation method used in our simulations is introduced. In Section III, simulated results of the fringing-field effects on reflective LCOS and transmissive TFT-LCD's are discussed. In Section IV, the CPVA concept for minimizing the fringing-field effects is presented. Finally, few conclusions on this study are drawn in Section V.

II. Extended Beam Propagation Method

Conventional matrix-type optical simulation methods are based on the assumption of a stratified medium, which allows the LC directors vary only in the light propagating direction. Therefore, light scattering and diffraction effects are excluded. These methods are reliable only when the LC profiles are maintained uniformly over a scale far exceeding the optical wavelength.

In microdisplay devices, the pixel pitches are so small that the diffraction effects cannot be ignored. A two-dimensional (2-D) optical simulator must be employed in order to accurately analyze the optical performance of the LC panels [17]. The traditional BPM is quite useful for analyzing the transmissive microdisplay devices [18], [19]. We further extend the BPM to reflective LCOS devices by incorporating the mirror image concept [20].

To simulate the electro-optic performances of a LCOS panel, we first calculate the LC director profile using a commercial software package (*2dimMos* from Autronics), and then calculate the corresponding optical properties by the extended BPM

Manuscript received July 6, 2005; revised September 9, 2005. This work was supported by the National Science Council, R.O.C., under the Contract NSC 93-2112-M-009-022.

K.-H. Fan-Chiang was with Department of Photonics and Institute of Electro-Optical Engineering, National Chiao Tung University, Hsinchu 300, Taiwan, R.O.C. He is currently with Himax Technologies, Inc., Tainan 741, Taiwan, R.O.C. (simon_fc@himaxdisplay.com).

S.-T. Wu is with the College of Optics and Photonics, University of Central Florida, Orlando, FL 32816 USA (e-mail: swu@mail.ucf.edu).

S.-H. Chen is with the Department of Photonics and Institute of Electro-Optical Engineering, National Chiao Tung University, Hsinchu 300, Taiwan, R.O.C. (e-mail: shuhchen@mail.nctu.edu.tw).

Digital Object Identifier 10.1109/JDT.2005.858930

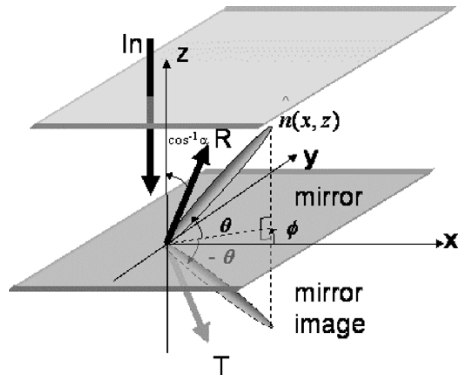

Fig. 1. Sketch of the angle definitions and the mirror image of the LCOS device.

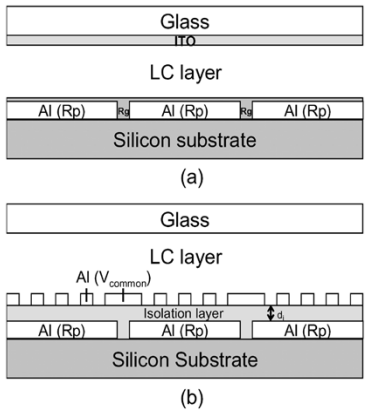

Fig. 2. Cell structures used for the 2-D computer simulations of: (a) MTN, TN, and VA modes (b) FOP mode.

with the finite difference algorithm. It starts with solving the Maxwell's curl equations discretely:

$$\nabla \times H = j\omega\varepsilon(x,z)E \tag{1}$$

$$\nabla \times E = -j\omega\mu_0 H. \tag{2}$$

Here, ω is the angular frequency, μ_0 is the permeability of vacuum, and the spatially dependent dielectric constant $\varepsilon(x,z)$ is the nine-element tensor related to the orientation of the local LC directors [3]. The differential equations are solved by the Crank-Nicolson scheme [18]. The transparent boundary condition (TBC) [21] is employed to avoid artificial reflections from the boundary. Finally, we obtain a sparse linear system [19]:

$$\begin{bmatrix} [M_{11}(\theta,\phi)] & [M_{12}(\theta,\phi)] \\ [M_{21}(\theta,\phi)] & [M_{22}(\theta,\phi)] \end{bmatrix} \begin{bmatrix} [E_y^{s-1}] \\ [H_y^{s-1}] \end{bmatrix} = \begin{bmatrix} [C_1(E_y^s, H_y^s)] \\ [C_2(E_y^s, H_y^s)] \end{bmatrix}. \tag{3}$$

Each of the sub-blocks $[M_{\mathrm{i,j}}]$ with $\mathrm{i,j} = 1,2$ corresponds to a tridiagonal matrix. Superscript $s = 1,2,\ldots \mathrm{n}$ indicates the propagation step of the discretized axial plane. E_y and H_y are the electric and magnetic fields in the y direction, respectively. Both C_1 and C_2 are functions related to E_y^s and H_y^s. By solving (3) with an initial condition of a plane wave propagating along the z direction, we obtain information that includes the amplitude and phase of the propagating light wave.

The reflective propagation process of the light wave can be derived by sending the light into the mirror image of the LC director distribution, as shown in Fig. 1. Therefore, the reflective transverse fields, $E_{ry}$and H_{ry}, of the LCOS device can be described as follows:

$$\begin{bmatrix} [M_{11}(-\theta,\phi)] & [M_{12}(-\theta,\phi)] \\ [M_{21}(-\theta,\phi)] & [M_{22}(-\theta,\phi)] \end{bmatrix} \begin{bmatrix} [E_{\mathrm{ry}}^{s+1}] \\ [H_{\mathrm{ry}}^{s+1}] \end{bmatrix} = \begin{bmatrix} [I_3(E_{\mathrm{ry}}^s, H_{\mathrm{ry}}^s)] \\ [I_4(E_{\mathrm{ry}}^s, H_{\mathrm{ry}}^s)] \end{bmatrix}. \tag{4}$$

The reflected fields polarized in the x and z directions (i.e., E_{rx} and E_{rz}) can be derived from (1)

$$E_{\mathrm{rx}} = -\frac{1}{j\omega\varepsilon_0\varsigma}\left(\varepsilon_{zz}^* \frac{\partial H_{\mathrm{ry}}}{\partial z} + \varepsilon_{xz}^* \frac{\partial H_{\mathrm{ry}}}{\partial x}\right) - \frac{\xi}{\varsigma} E_{\mathrm{ry}} \tag{5}$$

$$E_{\mathrm{rz}} = \frac{1}{j\omega\varepsilon_0\varsigma}\left(\varepsilon_{xx}^* \frac{\partial H_{\mathrm{ry}}}{\partial x} + \varepsilon_{zx}^* \frac{\partial H_{\mathrm{ry}}}{\partial z}\right) - \frac{\zeta}{\varsigma} E_{\mathrm{ry}} \tag{6}$$

where

$$\varsigma = \varepsilon(x,z)_{11}\varepsilon(x,z)_{33} - \varepsilon(x,z)_{31}\varepsilon(x,z)_{13},$$
$$\zeta = \varepsilon(x,z)_{11}\varepsilon(x,z)_{32} - \varepsilon(x,z)_{31}\varepsilon(x,z)_{12},$$
$$\xi = \varepsilon(x,z)_{12}\varepsilon(x,z)_{33} - \varepsilon(x,z)_{32}\varepsilon(x,z)_{13}.$$

The subscripts denote the indices of the dielectric tensor. Through (4) and (5), we can obtain the intensity of the signal light.

Fig. 2(a) shows the structure used for 2D simulations of MTN, TN, and VA modes. The pixel size is assumed to be 15 μm and the inter-pixel gap is 0.9 μm. The cell gap is adjusted to obtain the required $d\Delta n$ for each mode, where d is the cell gap and Δn is the LC birefringence. Fig. 2(b) shows the structure used for 2-D simulations of the FOP mode. The pixel size is 15.5 μm and the inter-pixel gap is 0.7 μm. Table I lists the LC parameters used for simulations. Here, we assume the reflectance of the reflective pixels is $\mathrm{Rp} = 1$ and the inter-pixel gap $\mathrm{Rg} = 0$. The pretilt angle is 2° for the MTN, TN, and FOP cells, and 88° for the VA cell. For all the following simulations, unless specifically mentioned, the incident light is assumed to be $\lambda = 540$ nm.

III. Fringing-Field Effects

In this section, we analyze the fringing-field effects of six commonly used LC modes for reflective LCOS microdisplays. For completeness, we also investigate the influences of the fringing fields on the transmissive TFT-LCDs, including TN and VA cells. The reflectance profile is calculated by BPM when the panel is operated at the dark-bright-dark state, which has the strongest lateral field component near the pixel edges.

A. Reflective LCOS Microdisplays

1) NW 90°-MTN Mode: This mode has twist angle $\Phi = 90°$ and the angle between the entrance LC director and the transmission axis of the polarizer $\beta = 20°$. The required phase retardation $d\Delta n$ is about 240 nm for normally white operation. Fig. 3(a) shows the simulated reflectance profile under crossed-polarizer condition when the panel is operated at the dark-bright-dark pixel configuration with 2.8 μm cell gap. The dark-state voltage is 5 $\mathrm{V_{rms}}$ and the bright-state voltage is 0.7 $\mathrm{V_{rms}}$. The fringing fields penetrating into the dark pixel areas cause unwanted rotation of the LC directors. Hence, light

TABLE I
LC AND CELL PARAMETERS USED FOR THE SIX MODES COMPARED IN OUR SIMULATIONS. THE UNIT OF K_{ii} IS pN AND $d\Delta n$ IS nm

	90°-MTN	45°-MTN	45°-TN	FCH	VA	FOP
K_{11}	13.1	13.1	13.9	13.4	16.7	16.7
K_{22}	10	10	10	6	7	7
K_{33}	22.3	22.3	21.5	19	18.1	18.1
$d\Delta n$	240	195	533	184	192	207.5
$\varepsilon_{\parallel}$	10.1	10.1	10.5	10.5	3.6	3.6
$\varepsilon_{\perp}$	3.3	3.3	3.5	3.6	7.8	7.8

leakage is observed near the pixel edge, which reduces the contrast ratio and the image sharpness as shown in Fig. 3(a). On the other hand, since $Rg \neq Rp$, some optical fringes exist near the pixel edges due to interferences. These results are similar to the Fresnel diffraction patterns induced by a straightedge.

The advantages of the 90°-MTN mode are twofold: 1) a high contrast ratio because of the built-in phase compensation of the two orthogonal boundary layers and 2) the relatively small fringing-field effects. However, its shortcoming is the reduced reflectivity. The calculated optical fill factor is only ~80% at the dark-bright-dark state. Here we define the optical fill factor as

$$F = \frac{1}{S}\int R_{\mathrm{bright}} \tag{7}$$

where S denotes the dimension of the pixels and $\mathrm{R_{bright}}$ is the normalized reflectance within the bright pixel area. Decreasing the twist angle could boost the optical fill factor, however, the contrast ratio decreases unless a thin phase compensation film is employed.

2) NW 45°-MTN Mode: The 45°-MTN cell has $\Phi = 45°$ and $\beta = 78°$. The required phase retardation $d\Delta n$ is 195 nm for normally white operation. In order to obtain a good dark state at low voltage, a uniaxial phase compensation film is applied. The angle between the optical axis of the film and the entrance LC director is 110°, and the phase retardation required for the compensation film $(d\Delta n)_{\mathrm{film}} = 27$ nm. Fig. 3(b) plots the 2D simulation results of the reflectance profile for the dark-bright-dark pixel configuration with 2.3 μm cell gap. The dark-state voltage is 5 $\mathrm{V_{rms}}$ and the bright-state voltage is 0.7 $\mathrm{V_{rms}}$. Due to the low $d\Delta n$ value which, in turn, leads to a thin cell gap for the 45°-MTN cell, the fringing-field effect is suppressed and the light leakage is much weaker than that of the 90°-MTN cell. Another benefit of this mode from thin cell gap viewpoint is fast response time. Therefore, this mode is particularly attractive for color sequential displays using a single LCOS panel [5]. Moreover, the calculated optical fill factor is up to 97% which results in high image brightness. However, the dark state of this mode is not as good as that of 90°-MTN mode since the complete phase compensation only occurs in the vicinities of the designed central wavelength. Besides, the required compensation film has a relatively small $d\Delta n$ value which is not easy to fabricate. The film needs to be laminated onto the surface of the polarizing beam splitter. Any artifacts or bubbles during the lamination process would be magnified and projected to the screen. Moreover, the film has to withstand high flux illumination from the arc lamp. Its thermal stress and stress birefringence could be problematic.

3) NB 45°-TN Mode: This mode was first reported by Grinberg *et al.* [6]. The cell parameters are as follows: $\Phi = 45°, \beta = 0°$, and $d\Delta n = 533$ nm for NB operation. The large $\mathrm{d\Delta n}$ implies a large cell gap (or high Δn LC) is required, which leads to a strong fringing filed effect. The 2D simulated reflectance profile of the 45°-TN cell when operated at the dark-bright-dark state with $d = 5$ μm is plotted in Fig. 3(c). The dark-state voltage is 0.7 $\mathrm{V_{rms}}$ and the bright-state voltage is 2.8 $\mathrm{V_{rms}}$. As shown in Fig. 3(c), the whole bright area is shifted into the right-hand dark pixel due to the strong fringing-field effect. The image sharpness and the contrast ratio are hence deteriorated significantly. The calculated dark-bright-dark contrast ratio is only 50:1 and the optical fill factor is only 69%. Here the dark-bright-dark contrast ratio is defined as

$$\mathrm{CR} \equiv \frac{\int_S R_{\mathrm{bright}}}{\int_{S/2} R_{R-\mathrm{dark}} + \int_{S/2} R_{L-\mathrm{dark}}} \tag{8}$$

where $\mathrm{R_{R-dark}}$ and $\mathrm{R_{L-dark}}$ denote the reflectance within the right and left dark pixel, respectively. One can reduce the cell gap to minimize the fringing-field effect. By using a 2.2 μm cell gap, the calculated contrast is greater than 300:1 and the optical fill factor is increased to 84%; however, a high birefringence $(\Delta n = 0.24)$ LC material is necessary to meet such a thin cell gap requirement. High Δn LC mixtures usually have a higher viscosity and worse photo and thermal stabilities than the low Δn mixtures.

4) NW Film-Compensated Homogenous (FCH) Mode: Film-compensated homogeneous cell is another candidate for reflective projection displays [7]. The principal axis of the film is oriented orthogonal to the LC axis so that their phase retardations are subtractive. Fig. 3(d) plots the 2D simulated reflectance profile for a homogeneous cell with $d\Delta n = 184$ nm, $\beta = 45°$, and $(\mathrm{d\Delta n})_{\mathrm{film}} = 52$ nm. The on-pixel is set at 4 $\mathrm{V_{rms}}$ and the adjacent off pixels are set at 1.5 $\mathrm{V_{rms}}$. The cell gap $d = 1.5$ μm. As shown in the figure, the light leakages due to the fringing-field effect still appear in the vicinities of the dark pixels. Thus, the device contrast is reduced.

The major advantage of the FCH mode is its small $d\Delta n$ value. Using a thin cell gap leads to a reduced fringing-field effect and shorter response time. From Fig. 3(d), the calculated optical fill factor is 98%. However, the dark-bright-dark state contrast ratio is only 81:1 due to the light leakage caused by the fringing fields. Another drawback of the FCH mode is narrow range of dark-state voltage. In theory, the perfect compensation occurs only at a specific $d\Delta n$ value. Any deviation from this optimal value would cause the dark state voltage to drift. The LC

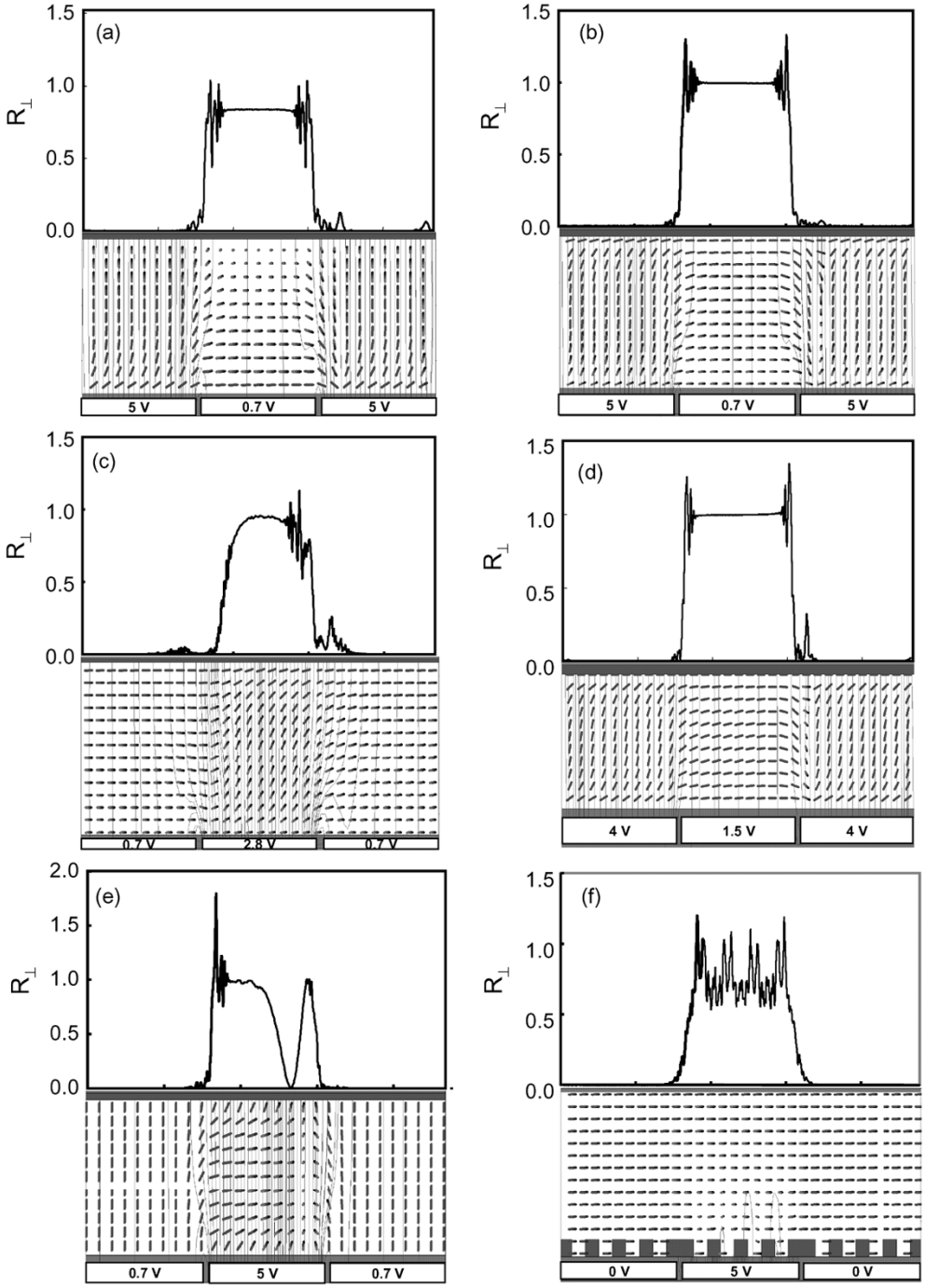

Fig. 3. Simulated results of the LC director distribution and reflectance profile by the extended BPM when the panel is operated at the dark-bright-dark state for: (a) 90°-MTN; (b) 45°-MTN; (c) 45°-TN; (d) FCH; (e) VA; and (f) FOP modes.

birefringence is more sensitive to temperature fluctuation than the compensation film. Thus, the $d\Delta n$ values of the LC and the compensation film should be designed at the expected operating temperature of the panel, say 55 °C. Using a film with a smaller $d\Delta n$ value broadens the dark state voltage, but the dark state would occur at a higher voltage.

5) NB Vertically Aligned (VA) Mode: In the VA mode, $\Phi = 0°, \beta = 45°$, and $d\Delta n = 192$ nm. The LC directors are aligned nearly perpendicular to the substrate surfaces, except for a small angle $(\sim 2°)$ deviated from the surface normal to create a preferred reorientation direction. The LC material employed should have a negative dielectric anisotropy. Since the residual phase of the dark state is very small, VA mode exhibits a very high contrast ratio under the crossed-polarizer condition. Moreover, the contrast ratio is relatively insensitive to the incident wavelength, cell gap, and operating temperature. Hence, VA mode is a favorite choice for LCOS applications.

Although VA mode has the abovementioned advantages, its fringing-field effect is rather strong. Fig. 3(e) plots the 2-D simulated dark-bright-dark reflectance profile with $d = 2.3\ \mu$m. The dark-state voltage is set at 0.7 V_{rms} and the bright-state voltage is 5 V_{rms}. As shown in the figure, the fringing fields induce a broad

dark stripe near the right edge of the bright pixels. This dark stripe splits the bright pixel into two unequal parts and drastically reduces the optical fill factor, which is ~70%. In addition, the LC distortions caused by the fringing fields even encumber the dynamic switching of the image and produce a very slow transition in the dynamic process, as will be discussed in Section IV.

It is noteworthy that by shrinking the cell gap and increasing the pretilt angle of the VA cell, e.g., 5–8° from vertical, the fringing-field-caused LC distortions can be reduced [22], [23]. For a thinner cell gap and larger pretilt angle, the dark stripe as observed in Fig. 3(e) becomes narrower and the decay time is shorter. However, the large pretilt angle causes an increased light leakage in the dark state. Some kind of phase compensation is necessary in order to restore the inherently high contrast ratio of the VA cell. An alternative method to eliminate the fringing-field effect will be given in Section IV.

6) NB Finger-on-Plane (FOP) Mode: The FOP mode was first developed by Chou *et al.* [9] to eliminate the fringing-field effect. Fig. 3(f) shows the 2D simulated reflectance profile of the FOP device when operated at the dark-bright-dark state with $\Phi = 0°, \beta = 0°$, and $d\Delta n = 207.5$ nm. The dark-state and bright-state voltages are 0 and 5 V_{rms}, respectively. The cell gap $d = 2.5$ μm. Recall that the FOP cell structure shown in Fig. 2(b), the comb-like common electrodes fabricated on the top of the pixel electrodes can effectively constrain the electric fields within the voltage-on pixel. Therefore, no light leakage is observed in the dark-pixel areas. However, the tiny common electrodes on the bottom substrate of the FOP device act as a phase grating. The light waves encountering these electrodes are scattered and diffracted at various angles. The light waves propagating outside the acceptance angle of the projection lens are wasted.

In order to investigate the diffraction effect of the FOP cell, it is important to calculate the angular distribution of the light intensity, which is called the intensity angular spectrum. After obtaining the information concerning the propagating fields from (4) and (5), the amplitude angular spectra, $A_{x,y}(\alpha/\lambda)$, of the transverse fields, E^n_{rx} and E^n_{ry} can be derived by using Fourier transform:

$$A_{x,y}\left(\frac{\alpha}{\lambda}\right) = \int E^n_{rx,ry} \exp\left[j2\pi \cos\left(\frac{\pi/2 - \cos^{-1}\alpha}{\lambda}x\right)\right] dx \tag{9}$$

where λ is the light wavelength in the propagation medium and α represents the cosine of the beam propagation direction depicted in Fig. 1. Finally, the output intensity angular spectrum is expressed as:

$$I\left(\frac{\alpha}{\lambda}\right) = A_x^2 + A_y^2. \tag{10}$$

Equation (10) represents the spectrum of the light at the end of the propagation prior to entering the cover glass. When the light exits the LC panel, the refractions at the interfaces of the cover glass and the air must be taken into consideration. As a consequence, the final propagation angle, θ_p, is given as follows:

$$\theta_p = \sin^{-1}\left(n^n_{eff} \times \sin(\cos^{-1}\alpha)\right) \tag{11}$$

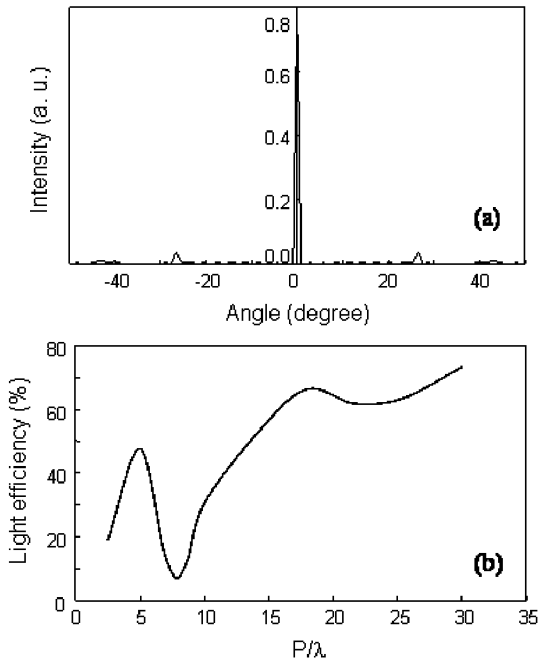

Fig. 4. Simulated results of the FOP LCOS devices in the voltage-off state by the extended BPM: (a) the intensity angular spectrum with $P = 15.5$ μm and $\lambda = 540$ nm, (b) the light efficiencies $(F_{\#} = 2.8)$ of the LCOS devices with respect to the P/λ value.

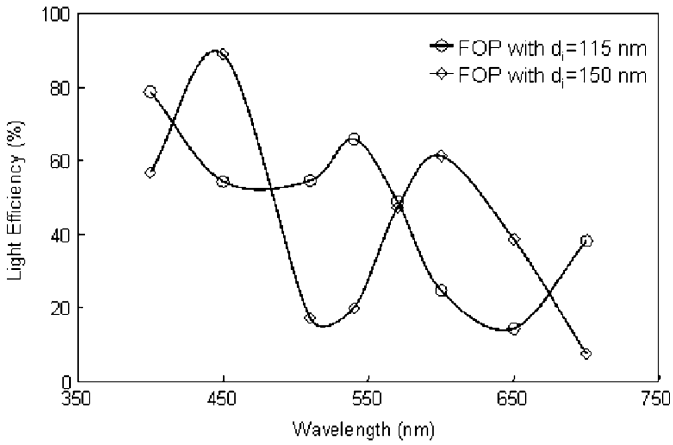

Fig. 5. Calculated light efficiency with respect to the wavelength for the FOP mode ($P = 15.5$ μm) with $d_i = 115$ nm and 150 nm.

where n^n_{eff} represents the effective refractive index at the end of the propagation in the LC layer. The light efficiency of the LCOS panels η is defined as follows:

$$\eta = \frac{\int_{-\theta_a}^{\theta_a} I\left(\frac{\theta_p}{\lambda}\right)}{I_{in}} \tag{12}$$

where $I_{in}$is the intensity of the incident light and θ_a represents the acceptance angle of the optical system which is related to the f-number $(F_{\#})$ of the system:

$$\theta_a = \tan^{-1}\left(\frac{1}{2F_{\#}}\right). \tag{13}$$

Fig. 4(a) shows the intensity angular spectrum calculated when all the pixels are turned off. It can be easily seen that significant portion of the light travels at angles above

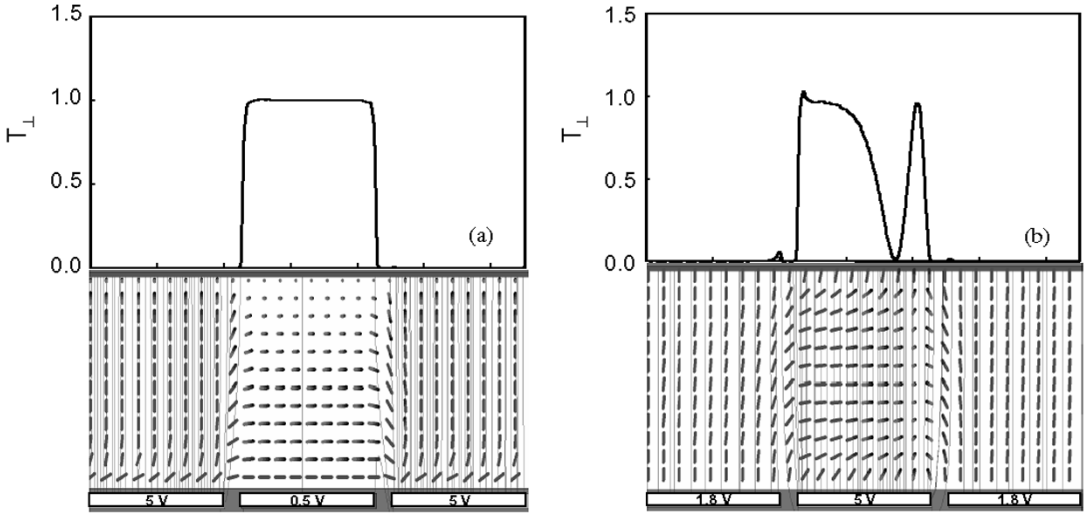

Fig. 6. Simulated results of the LC director distribution and transmittance profile by BPM when the panel is operated at the dark-bright-dark state for two transmission-type LC microdisplays. (a) 90°-TN cell. (b) VA cell.

TABLE II
COMPARISON OF THE OPTICAL PERFORMANCE OF EACH LC MODE WHEN OPERATED AT THE DARK-BRIGHT-DARK STATE

	90°-MTN	45°-MTN	45°-TN	FCH	VA	FOP
Optical Fill Factor (%)	80	97	69	98	71	63
Contrast Ratio	123	214	50	81	383	318
Others Issues		Needs a film		Needs a film	Slow dark-bright-dark to all-bright transition	Strong diffraction

$\pm 20°$ from the substrate normal. Fig. 4(b) plots the calculated light efficiencies of the FOP device with respect to the pitch-over-wavelength (P/λ) value using $F_{\#} = 2.8$, i.e., $\theta_{\mathrm{a}} = 10°$. As shown in the figure, the light loss due to the diffraction becomes unbearable as the pixel pitch is reduced. Even when $P/\lambda = 30$, which means $P = 16.2\,\mu$m for $\lambda = 540$ nm, the light loss is still more than 20%.

By appropriately adjusting the thickness of the isolation layer between the pixel and common electrodes (d_i), one can boost the light efficiency of the FOP device. For example, we simulated the light efficiency with respect to the wavelength for the FOP mode ($P = 15.5\,\mu$m) for different values of d_i, as shown in Fig. 5. From the figure, the green (G) band exhibits a higher efficiency at $d_{\mathrm{i}} = 115$ nm while the red (R) and blue (B) bands favor $d_i = 150$ nm. Therefore, the light efficiency of the FOP device can be enhanced in a two- or three-panel projection system by optimizing the value of d_i corresponding to the R, G, and B bands, respectively [3]. Even so, the overall light efficiency is still not very high.

B. Transmissive LC Microdisplays

In a transmissive microdisplay, the fringing-field effect is usually assumed to be negligible because of the large pixel pitch ($>20\,\mu$m) and the wide inter-pixel gap. However, this presumption no longer holds for the LC panels using a negative $(\Delta\varepsilon < 0)$ LC mixture. Fig. 6(a) and (b) shows the simulated 2-D transmittance profiles of the TN and VA cells, respectively. The pixel size is 40 μm and the inter-pixel gap is 5 μm. The $d\Delta n$ is 477.5 nm for the TN cell and 382 nm for the VA cell. As shown in Fig. 6(a), indeed, the transmittance profile is almost perfect for the TN cell. The calculated optical filled factor is as high as 99% and the dark-bright-dark contrast ratio exceeds 1000:1. On the contrary, the optical performance of the transmissive VA cell is severely deteriorated due to the fringing-field effect despite the large pixel pitch and wide inter-pixel gap. The mechanism of this optical appearance is related to the negative LC material employed in the VA mode, which will be explained in next section.

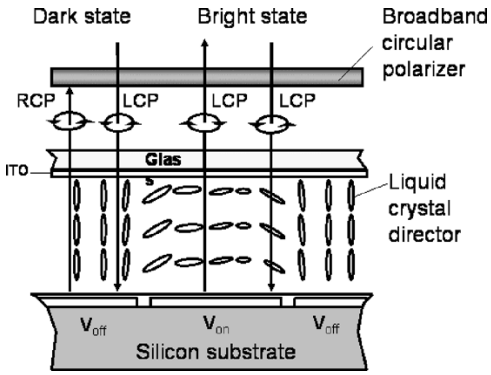

Fig. 7. Schematic drawing of the cell structure of the CPVA device.

IV. CIRCULARLY POLARIZED LIGHT ILLUMINATED VA LCOS DEVICE

The influences of the fringing-field effect in six commonly used LC modes have been discussed in the previous section. Table II summarizes the optical performances of each LC mode.

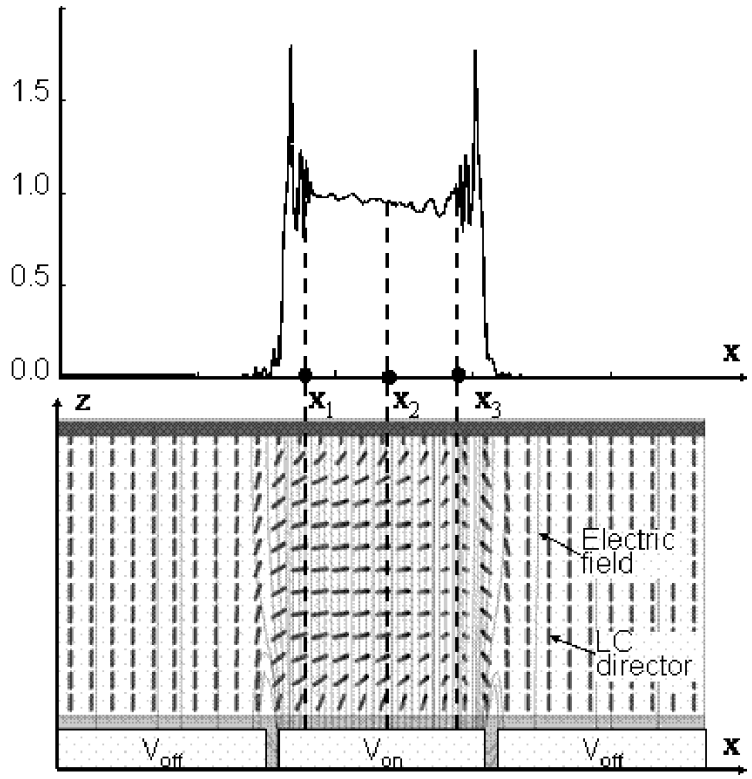

Fig. 8. The simulated LC director distribution and the corresponding reflectance profiles at the dark-bright-dark for the CPVA device. The on-state voltage $V_{\rm on} = 5\ {\rm V_{rms}}$ and the off-state voltage $V_{\rm off} = 0.7\ {\rm V_{rms}}$.

Among them, the VA LCOS is particularly promising because of its inherent high contrast ratio. However, the fringing-field -caused light loss is relatively high $(\sim 30\%)$ when a linearly polarized light in employed. Hence, the sharpness and brightness of the displayed images are deteriorated tremendously. Moreover, the optical transition time of the VA panel switched from the dark-bright-dark states to the all-bright state is extremely slow which results in blurred images [24], [25].

In this section, we describe a circularly polarized light illuminated vertical alignment (CPVA) liquid crystal cell which not only preserves the light in the presence of the lateral fringing field but also gives a fast optical switching time (<10 ms) to eliminate the blurring of the moving images. Fig. 7 depicts the cell configuration of the CPVA device. As shown in the figure, a broadband circular polarizer is placed on top of the LCOS panel. Therefore, the incident light is circularly polarized before entering the LC layer. After traversing through the LC layer twice, the light will be analyzed by the same circular polarizer and directed to the detector.

Fig. 8 depicts the 2-D simulated results of the LC director distribution and the corresponding reflectance profiles at the dark-bright-dark state for the CPVA systems. The calculated optical filled factor is 97% and the calculated dark-bright-dark contrast ratio is 487:1. Fig. 9 shows the simulated azimuthal angle (ϕ) of the LC directors along the z direction at the specified x positions, $\mathrm{x} = \mathrm{x}_1, \mathrm{x}_2, \mathrm{x}_3$ as denoted in Fig. 8. As shown in the figures, the largest polar angle appears near the middle plane because the negative type $(\Delta\varepsilon < 0)$ LC molecules tend to orient themselves perpendicular to the electric field [16]. Therefore,

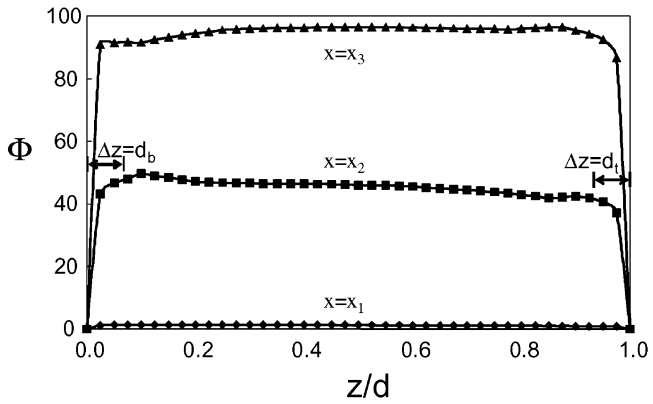

Fig. 9. Calculated twist angles (Φ) of the LC directors along the z direction at $\mathrm{x} = \mathrm{x}_1, \mathrm{x}_2$, and x_3 as denoted in Fig. 8.

the LC director profile can be regarded as a screw-like structure with its helical axis along z-axis and have opposite rotational sense in the upper and lower parts.

With regard to the optical properties, as shown in Fig. 8, the reflectance profile is not influenced by the director distortions in the x–y plane leading to a high sharpness and high brightness image. This unique optical property can be interpreted qualitatively by de Vries theory [26]. As mentioned above, the LC director profile can be regarded as a screw-like structure. Assuming a wave propagates along the helical axis of an ideal helical structure with a fixed pitch P_0. In general, there are two eigenwaves propagating in the same direction. Their eigenvalues $l_i, i = 1, 2$, satisfy the dispersion relation which can be

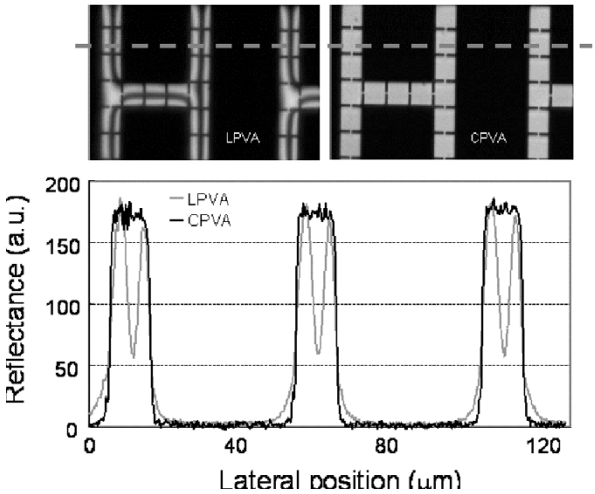

Fig. 10. The experimental results of the LPVA and CPVA devices captured by CCD through the polarizing microscope when operated at the dark-bright-dark pixel configuration. The normalized reflectance profiles were measured along the dashed line shown in the photos.

derived from solving the Maxwell's equations supplemented by the constitutive equation [27], [28]:

$$\left(-k_0^2 + l_i^2 + q_0^2\right)^2 - 4q_0^2 l_i^2 - k_1^4 = 0 \tag{14}$$

where $k_0^2 = (2\pi/\lambda)^2(n_e^2 + n_o^2)/2, k_1^2 = (2\pi/\lambda)^2(n_e^2 - n_o^2)/2, q_0 = 2\pi/P_0$ and λ is the wavelength of the incident light. n_e and n_o are the extraordinary and ordinary refractive index of the LC material. When P_0 and λ are known, one can obtain the ellipticity of the eigenwaves as:

$$\rho = \frac{2l_i q_0}{\pm\sqrt{k_1^4 + 4q_0^2 l_i^2} - k_1^2} \tag{15}$$

where $l_i = \sqrt{k_0^2 + q_0^2 \pm \sqrt{4k_0^2 q_0^2 + k_1^4}}$.

The optical behaviors of the circularly polarized light propagating in the VA cell can be understood easily by the above arguments with an approximated model, which is a nontwisted LC layer sandwiched between two twisted layers. In Fig. 9, the twisted regimes near the substrates ($0 \le \mathrm{z} \le \mathrm{d_b}$ and $\mathrm{d} - \mathrm{d_t} \le \mathrm{z} \le \mathrm{d}$) have their effective pitch $|\mathrm{P_0}| = [2\pi/\Phi(\mathrm{d_b})]\mathrm{d_b} \cong [2\pi/\Phi(\mathrm{d} - \mathrm{d_t})]\mathrm{d_t}$, where $\Phi(\mathrm{z})$ denotes the twist angle of the LC director at z and is defined as the difference of azimuthal angles between that LC director and the surface LC director. By using (15), the eigenwaves in these regimes are almost circularly polarized for the visible light. The incident circularly polarized light remains its polarization state after passing the top-twisted regime. Note that a circularly polarized light can be regarded as the superposition of any two orthogonal linearly polarized waves with the same amplitude and $\pi/2$ phase difference. The nontwisted uniform regime ($\mathrm{d_b} < \mathrm{z} < \mathrm{d} - \mathrm{d_t}$) with linearly polarized eigenwaves provides a phase difference, say $\delta = \pi/2$, such that the resulted light is linearly polarized in the direction at 45° from the local LC director $\mathbf{n}$. The reflected light that traverses through the bottom-twisted regime twice (forward and backward) will have the same linear polarization. Then the uniform regime changes it to be circularly polarized by gathering another $\pi/2$ phase change. The polarization state of the outgoing circular wave will again not be influenced after traversing through the top-twisted regime. Finally, almost all of the light passes through the broadband circular polarizer. In other words, the CPVA system preserves the input light efficiently.

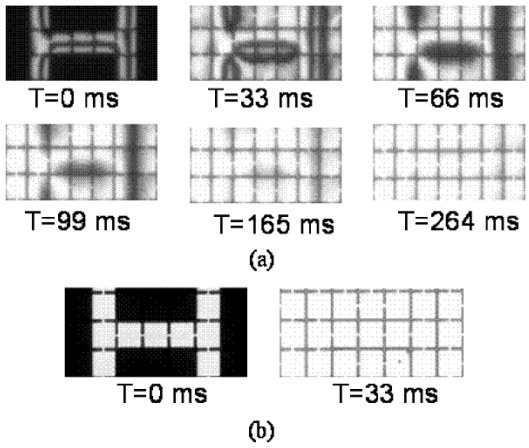

Fig. 11. Photos capture by CCD through polarizing microscope of the LC panel after switching from the dark-bright-dark state to the all-bright state for: (a) the LPVA device and (b) the CPVA device. T is the elapsed time after switching.

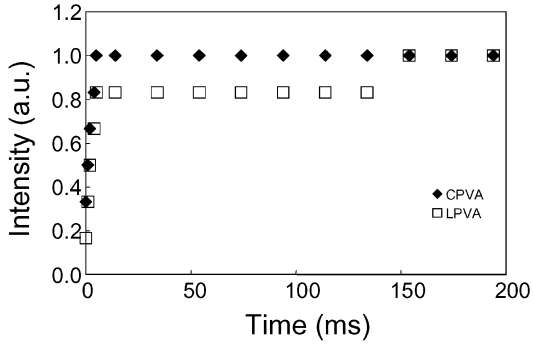

Fig. 12. Measured reflectance with respect to the elapsed time after switching from the dark-bright-dark state to the all-bright state for the CPVA and the LPVA devices.

Fig. 10 shows the experimental results of the CPVA and the conventional VA using linearly polarized light (LPVA) operated at the dark-bright-dark pixel configuration. The photos were captured by CCD through the polarizing microscope. The two-dimensional normalized reflectance profiles, which were measured along the dashed lines shown in the photos, are also shown in this figure. It is clearly shown that the image of the LPVA device is degraded by the fringing-field effect severely. The dark lines in the bright pixels originate from the distortion of the LC director profile as simulated in Fig. 3(e). On the contrary, the CPVA device is free from the dark lines, which agrees with our simulated results very well. Therefore, the sharpness and the brightness of the displayed images are enhanced significantly.

The CPVA optical system not only improves the static performance but also dramatically reduces the dynamic response time of the LCOS panel. Figs. 11(a) and (b) show the photos of the LC panel switched from the dark-bright-dark state to the all-bright state for the LPVA and the CPVA devices, respectively. The distorted LC directors take hundreds of milliseconds to relax back to their original state. As a result, the dark lines in the LPVA device last over 150 ms after switching, which cause a serious

image blurring. Since the distorted LC directors are mainly rotating in the x-y plane during the relaxation process, the effect of the slow relaxation to the optical response of the CPVA device is very small as shown in Fig. 11(b). Fig. 12 shows the measured reflectance with respect to the elapsed time after switching from the dark-bright-dark state to the all-bright state for both CPVA and LPVA devices. Results indicate that the transition time of the CPVA device is actually less than 10 ms [16].

It is noteworthy that the polarization states of the incident light and the reflected light are identical in the CPVA system, which means the lights can not be separated by the polarizing beam splitter (PBS). Therefore, the optical engine must be designed without using any PBS. An example of such optical engines is the off-axis system [29]. The off-axis system has the propagating direction deviates from the substrate normal with a small angle. In this condition, compensation films are required in order to obtain a good dark state, which may increase the manufacturing cost. Moreover, the optical engine may be too complicated and not practical for mass production. Another solution is to use polarization-independent beam splitter (BS) to separate the incident and the signal lights [30]. However, $3/4$ light energy will be wasted after passing through the BS twice, which results in a poor light efficiency. The holographic film developed by JVC [31] is another solution to the CPVA system. The incident light propagating in a certain direction will be directed to the LCOS panel due to the Bragg's diffraction [32]. After being modulated by the LC layer, the signal light will pass through the film again without deflection. One can use the three-panel system to release the alignment difficulties of the holographic film incurred in the one-panel system [32]. The main consideration is the diffraction efficiency of the holographic film, which directly affects the light efficiency of the optical system.

V. Conclusion

The fringing-field effects of six commonly used LC modes for LCOS devices are analyzed by the rigorous beam propagation method. The 90°- and 45°-MTN modes exhibit a weaker fringing-field effect because of the smaller cell gap, but the optical fill factor of the 90°-MTN mode is only $\sim$80% which results in a reduced brightness. For the 45°-MTN, a uniaxial compensation film is required in order to obtain a good dark state at a low voltage, which increases the manufacturing cost. Thermal-induced stress and birefringence of the film need to be considered as well. On the 45°-TN mode, the fringing-field effects are strong due to the thick cell gap. Reducing cell gap will effectively suppress the fringing-field effect, however, high birefringence materials need to be used to satisfy the large $d\Delta n$ requirement. High birefringence LC mixtures usually have a higher viscosity and less photo and thermal stabilities. For the film-compensated homogenous cell, a compensation film is applied to reduce the residual phase originating from the boundary LC directors. Although it has a very high optical fill factor, the fringing-field-induced light leakage reduces the contrast ratio significantly. With regard to the VA mode, the excellent dark state in the voltage-off condition makes it a favorable choice for projection displays. The main problem of the VA mode is the severe fringing-field effect which produces a broad dark stripe in the bright pixels. Such effect not only decreases the image sharpness and brightness, but also causes image blurring when the panel is switched from the dark-bright-dark state to the all-bright sate. When considering the FOP mode, its optical performance is not influenced by the fringing-field effect, however, the comb-like common electrodes induce severe diffraction effect which causes unbearable light loss. By appropriately adjusting the thickness of the isolation layer between the pixel electrode and the common electrode, the light efficiency can be enhanced significantly.

In a transmissive microdisplay using a TN cell, the fringing-field effect is much weaker than that in the reflective LCOS displays. The projection optics for a transmissive display is simpler, but its response time is slower because of the higher $\mathrm{d}\Delta\mathrm{n}$ value required. When using a negative LC material in a VA cell, the optical performance is still severely degraded by the fringing fields, similar to that of a VA-LCOS.

In order to eliminate the fringing-field effect in the VA device, the circularly polarized light illuminated VA LCOS microdisplay is introduced. It is shown that the image sharpness and the brightness of the panel are dramatically improved. In addition, the dynamic transition time of the device switched from the dark-bright-dark states to the all-bright state is less than 10 ms, which sufficiently overcomes the image blurring effect. The optical properties are interpreted qualitatively by the de Vries theory. Potential applications of this device for high contrast and high brightness reflective LCOS and transmissive p-Si TFT-LCD projection displays are foreseeable.

References

[1] E. H. Stupp and M. S. Brennesholtz, *Projection Displays*. New York: Wiley, 1998.

[2] Y. Ji, J. Grandhi, and M. E. Stefanov, "Fringing-field effects in reflective CMOS LCD," in *Soc. Inf. Display Tech. Dig.*, vol. 30, May 1999, pp. 750–753.

[3] K. H. F. Chiang, S. H. Chen, and S. T. Wu, "Diffraction effect on the high resolution liquid-crystal-on-silicon devices," *Jpn. J. Appl. Phys.*, vol. 44, pp. 3068–3072, May 2005.

[4] S. T. Wu and C. S. Wu, "Mixed-mode twisted nematic liquid crystal cells for reflective display," *Appl. Phy. Lett.*, vol. 68, pp. 1455–1457, Mar. 1996.

[5] P. Janssen, J. A. Shimizu, J. Dean, and R. Albu, "Design aspects of a scrolling color LCoS display," *Displays*, vol. 23, pp. 99–108, 2002.

[6] J. Grinberg, A. Jacobson, W. Bleha, L. Boswell, and G. Myer, "New real-time noncoherent to coherent light image converter- hybrid field-effect liquid-crystal light valve," *Opt. Eng.*, vol. 14, pp. 217–225, Mar. 1975.

[7] S. T. Wu and C. S. Wu, "A biaxial film-compensated thin homogenous cell for reflective liquid crystal display," *J. Appl. Phys.*, vol. 83, pp. 4096–4100, Apr. 1998.

[8] M. F. Schiekel and K. Fahewnschon, "Deformation of nematic liquid crystals with vertical orientation in electric fields," *Appl. Phys. Lett.*, vol. 19, pp. 391–393, Nov. 1971.

[9] W. Y. Chou, C. H. Hsu, S. W. Chang, H. C. Chiang, and T. Y. Ho, "A novel design to eliminate fringe field effects for liquid crystal on silicon," *Jpn. J. Appl. Phys.*, vol. 41, pp. 7386–7390, Dec. 2002.

[10] R. C. Jones, "A new calculus for the treatment of optical systems I. Description and discussion of the calculus," *J. Opt. Soc. Amer.*, vol. 31, pp. 488–493, July 1941.

[11] D. W. Berreman, "Optics in stratified and anisotropic media—4×4-matrix formulation," *J. Opt. Soc. Amer.*, vol. 62, pp. 502–510, Apr. 1972.

[12] A. Lien, "Extended Jones matrix representation for the twisted nematic liquid-crystal display at oblique-incidence," *Appl. Phys. Lett.*, vol. 57, pp. 2767–2769, Dec. 1990.

[13] B. Witzigmann, P. Regli, and W. Fichtner, "Rigorous electromagnetic simulation of liquid crystal displays," *J. Opt. Soc. Amer. A*, vol. 15, pp. 753–757, Mar. 1998.

[14] E. E. Kriezis and S. J. Elston, "Finite-difference time domain method for light wave propagation within liquid crystal devices," *Opt. Commun.*, vol. 165, pp. 99–105, July 1999.
[15] ——, "Light wave propagation in liquid crystal displays by the 2-D finite-difference time-domain method," *Opt. Commun.*, vol. 177, pp. 69–77, Apr. 2000.
[16] K. H. F. Chiang, S. T. Wu, and S. H. Chen, "High-definition vertically-aligned liquid crystal microdisplays using a circularly polarized light," *Appl. Phys. Lett.*, vol. 87, p. 031 110, Jul. 2005.
[17] D. A. Yakovlev, V. I. Tsoy, and V. G. Chigrinov, "Advanced Tools for Modeling of 2D-Optics of LCDs," in *Soc. Inf. Display Tech. Dig.*, vol. 36, May 2005, pp. 58–61.
[18] E. E. Kriezis and S. J. Elston, "A wide angle beam propagation method for the analysis of tilted nematic liquid crystal structures," *J. Mod. Opt.*, vol. 46, pp. 1201–1212, Jul. 1999.
[19] ——, "Wide-angle beam propagation method for liquid-crystal device calculations," *Appl. Opt.*, vol. 39, pp. 5707–5714, Nov. 2000.
[20] S. T. Wu and D. K. Yang, *Reflective Liquid Crystal Displays*. New York: Wiley, 2001.
[21] G. R. Hadley, "Transparent boundary condition for the beam propagation method," *IEEE J. Quantum Electron.*, vol. 28, no. 1, pp. 363–370, Jan. 1992.
[22] D. Cuypers, H. De Smet, and A. Van Calster, "Fringing-field induced Disclinations in VAN LCoS Panels," in *Int. Display Workshop*, 2004, pp. 1679–1682.
[23] ——, "Fringing field effects in microdisplays," in *Soc. Inf. Display Tech. Dig.*, vol. 36, May 2005, pp. 1298–1301.
[24] S. Zhang, M. Lu, and K. H. Yang, "Direct observation of disclination evolution in vertically aligned liquid crystal light valves," in *Soc. Inf. Display Tech. Dig.*, vol. 31, May 2000, pp. 898–902.
[25] M. Lu and K. H. Yang, *Asian Soc. Inf. Display Tech. Dig.*, vol. 31, Oct. 2000, pp. 30–33.
[26] H. de Vries, "Rotatory power and other optical properties of certain liquid crystals," *Acta Crystallogr.*, vol. 4, pp. 219–226, Mar. 1951.
[27] P. G. de Gennes and J. Prost, *The Physics of Liquid Crystals*. Oxford, U.K.: Clarendon Press, 1993.
[28] P. C. Yeh and C. Gu, *Optics of Liquid Crystal Displays*. New York: Wiley, 1999.
[29] B. A. Scott and W. L. DeBoynton, "Light Separation and Recombination System for an Off-Axis Projector," U.S. Patent 6 046 858, Apr. 2000.
[30] J. E. Anderson, J. Gandhi, and M. E. Stefenov, "PH-VAN system design for high contrast rub-free microdisplays," in *Soc. Inf. Display Tech. Dig.*, vol. 32, May 2001, pp. 340–343.
[31] T. Yamazaki, M. Tokumi, T. Suzuki, S. Nakagaki, and S. Shimizu, "The single-panel D-ILA hologram device for ILA™ projection TV," in *Int. Display Workshop*, 2000, pp. 1077–1080.
[32] H. Kogelnik, "Couple wave theory for thick hologram grating," *Bell. Syst. Tech. J.*, vol. 48, pp. 2909–2947, 1969.

Kuan-Hsu Fan-Chiang received the Ph.D. degre from the Institute of Electro-optical Engineering, National Chiao Tung University, Taiwan, R.O.C., in 2005.

From 2003 to 2004, he spent a year at University of Central Florida, orlando, as an exchange student. Since October 2005, he has been with Himax Technologies Inc., Tainan, Taiwan, R.O.C. His research activities focus on modeling of liquid-crystal-on-silicon (LCOS) panels for projection displays, especially in the investigations of fringing field and diffraction effects of high-definition LCOS panels.

Shin-Tson Wu (M'98–SM'99–F'04) received the B.S. degree in physics from National Taiwan University, and the Ph.D. degree from the University of Southern California, Los Angeles.

He is currently a PREP professor at College of Optics and Photonics, University of Central Florida (UCF), Orlando. Prior to joining UCF in 2001, he worked at Hughes Research Laboratories, Malibu, CA, for 18 years. His studies at UCF concentrate in foveated imaging, bio-photonics, optical communications, liquid crystal displays, and liquid crystal materials. He has coauthored 2 books, *Reflective Liquid Crystal Displays* (New York: Wiley, 2001) and *Optics and Nonlinear Optics of Liquid Crystals* (Singapore: World Scientific, 1993), 4 book chapters, and over 220 journal papers.

Dr. Wu is a Fellow of the Society for Information Display (SID) and Optical Society of America (OSA).

Shu-Hsia Chen received the B.S. degree in physics from the National Taiwan Normal University, Taiwan, R.O.C., in 1968 , the M.S. degrees in physics from North Carolina State University, Raleigh, NC, in 1970, and the M.S. degree in bionucleonics from Purdue University, West Lafayette, in 1973.

From 1974 to 2005, she has been a member of the faculty at National Chiao Tung University, Taiwan, R.O.C., , where she is currently a Professor Emeritus of the Institute of Electro-Optical Engineering.

Ms. Chen served as a member of the Board Directors of the International Liquid Crystal Society from 1992 to 2000. She was the President of ROC Taiwan Liquid Crystal Society from 1999 to 2003.